Journal of the European Ceramic Society 17 (1997) 1813–1818
© 1997 Elsevier Science Limited
Printed in Great Britain. All rights reserved
PII: S0955-2219(97)00064-2
0955-2219/97/$17.00 + 0.00

A New Class of Inorganic Compounds Containing Dinitrogen-Metal Bonds

L. Le Gendre, R. Marchand and Y. Laurent

Laboratoire des 'Verres et Céramiques', UMR 6512 CNRS,Université de Rennes I, 35042 Rennes, Cedex, France.

Abstract

TGA of particular oxynitrides shows an unexpected intermediate phase between starting oxynitride and final oxide. Transition between this intermediate phase and the oxide step, studied by high resolution mass spectrometry, reveals that this phenomenon can be ascribed to a nitrogen retention. We deduce the general formulation $M^{n+}O_{n/2}N_x$. *Particular properties of those phases are: low density, structure type analogous to the one of their oxynitride precursor and a nitrogen binding energy, measured by XPS, near 403 eV. By comparison to the binding energy range of organometallic dinitrogen complexes, we assume the presence of* $M–N{\equiv}N–M$ *entities included in an oxide lattice with cationic defect structure.*
© *1997 Elsevier Science Limited.*

Résumé

Le suivi de l'oxydation d'un certain nombre d'oxynitrures par analyse thermogravimétrique sous air (ATG) a révélé l'existence d'une phase intermédiaire inattendue entre le stade oxynitrure initial et le stade oxyde. La transition, sous atmosphère inerte à haute température, entre cette phase intermédiaire et l'oxyde se traduit par une importante perte de masse. Nous avons montré par spectrométrie de masse haute résolution, que ces phases étaient caractérisées par une rétention d'azote et pouvaient se formuler: $M^{n+}O_{n/2}N_x$. *Ceci se traduit par un degré d'oxydation formel de l'azote proche de zéro. Ces phases intermédiaires sont toutes caractérisées par une densité faible, un type structural similaire à celui de leur oxynitrure précurseur ainsi qu'une énergie de liaison de l'azote, mesurée par XPS, proche de 403 eV. Cette caractéristique XPS induit, par comparaison avec les gammes d'énergie de liaison de l'azote de complexes organométallique diazotés, l'existence d'entités* $M–N{\equiv}N–M$ *en interaction avec une matrice oxyde hautement lacunaire.*

1 Introduction

This paper describes and characterizes a so-called 'intermediate phase' phenomenon which has been evidenced in oxidation of different types of oxynitrides.[1–4]

When heated in an oxygen atmosphere, a nitride-type compound, either a nitride or an oxynitride, is systematically transformed at more or less high temperature into an oxide, or mixture of oxides, with nitrogen release as molecular dinitrogen. The reaction results in a gain in weight which is represented in Fig. 1(a) by a 'normal' curve of thermogravimetric analysis (TGA). However, some oxynitrides show different behavior under similar conditions. As illustrated by the TGA curve (b) of Fig. 1, an intermediate state appears between starting oxynitride and final oxide, with an associated weight gain surprisingly higher than that corresponding to the transformation into oxide. It concerns a nitrogen retention and the corresponding 'intermediate phases' have been isolated and characterized as a new class of nitrogen-containing inorganic compounds.

The present work deals with the preparation of eight different 'intermediate phases' from oxynitrides belonging to different structure types. Structure of these phases has been studied by XRD, density measurements and XPS. A structural model is presented and discussed.

2 Experimental

2.1 Precursor oxynitrides

Table 1 gathers the studied oxynitride compositions as well as the reference of their synthesis conditions. They were generally prepared by thermal nitridation in flowing ammonia of corresponding oxide. The compositions were deduced both from chemical analysis of nitrogen and

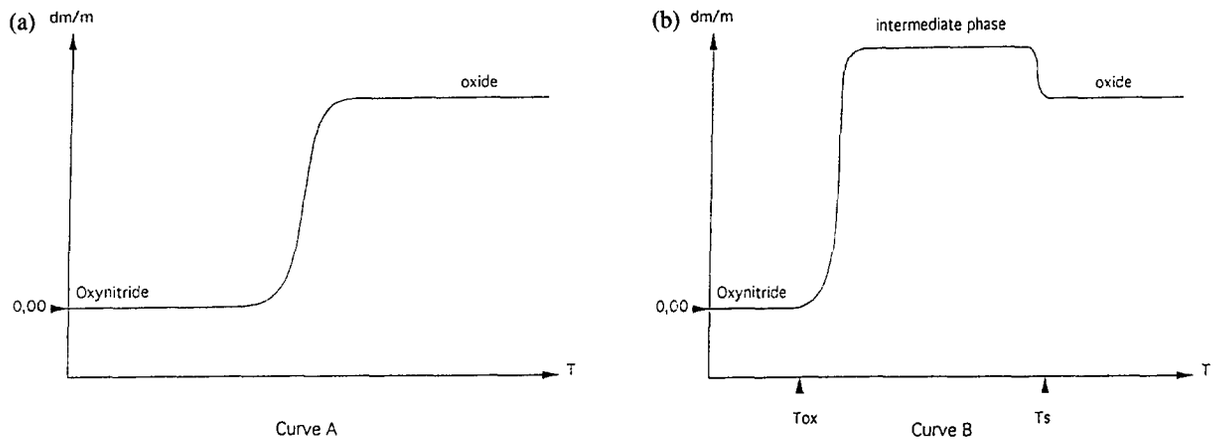

Fig. 1. TGA types (a) and (b) encountered during different oxynitride oxidations.

oxygen by the LECO method and from TGA results after total transformation into oxide.

2.2 Thermogravimetric analysis (TGA)

The oxidation behavior of the different oxynitride phases was investigated with a thermobalance Setaram TGDTA 92 in the room–1400°C temperature range. The samples were tested in static air (P = 1 atm) with constant heating rates always lower than 1·00 K mn^{-1}. The phases present after oxidation were identified by powder X-ray diffraction (XRD).

2.3 Density measurements

Density measurements were performed by pycnometric method using tetrachloromethane. First, powder was degassed under a vacuum of 1·3 Pa over a 2 h period. Before bringing it back to atmospheric pressure, the sample was recovered by CCl_4 in order to prevent air contact.

2.4 X-ray photoelectron spectroscopy (XPS)

The XPS measurements were performed on an SSI model 206 spectrometer (Surface Science Instrument) equipped with a monochromatic Al Kα X-ray source (1486·6 eV). More experimental details are given elsewhere.[4] The reported binding energies are referenced to the C_{1s} peak at 284·8 eV.

Table 1. Composition and structure type of the studied oxynitrides

Composition	*Structure type*	*Ref.*
$BaTaO_2N$	perovskite	5
$La_{0.91}W_{0.91}\square_{0.18}O_{1.37}N_{1.63}$	perovskite	6
$LaTiO_2N$	perovskite	7
$Al_{2.85}\square_{0.15}O_{3.45}N_{0.55}$	spinelle	1
$Y_{2.67}W_{1.33}(O_{3.79}N_{2.80}\square_{1.41})$	fluorite	8
$Cr_{0.77}\square_{0.23}O_{0.69}N_{0.31}$	NaCl	9
$Ti_{0.67}\square_{0.33}O_{0.42}N_{0.58}$	NaCl	4
$Nb_{0.54}\square_{0.46}O_{0.4}N_{0.6}$	NaCl	10

3 Intermediate Phase Phenomenon

Oxidation TGA curves of $LaTiO_2N$(a), $Y_{2.67}W_{1.33}O_{3.79}N_{2.80}\square_{1.41}$ (b), $BaTaO_2N$ (c), $Nb_{0.54}\square_{0.46}O_{0.4}N_{0.6}$ (d) are presented in Fig. 2.

Considering first the total weight gain, such thermogravimetric experiments are represented by the very general equation: $MO_xN_y + (z-x)/2\ O_2 \rightarrow MO_z + y/2\ N_2\uparrow$, where the oxidation state of M is (2x + 3y) in the starting oxynitride phase and 2z in the final oxide. Nitrogen is always released in molecular form. No other nitrogen species, such as NO/NO_x for example, has ever been detected. By way of illustration, when 2x + 3y = 2z, i.e. when the M oxidation state is the same before and after the 'oxidation' reaction, the oxynitride → oxide transformation corresponds to the substitution of $3O^{2-}$ for $2N^{3-}$, resulting in a total weight gain of 19·9848 g per released N_2 mole.

On the other hand, the mass variation with temperature shows, for every oxynitride presented in Table 1, an intermediate phase phenomenon associated, as will be shown below, to a nitrogen retention. Isothermal graphs, at temperatures deduced from TGA curves, clearly demonstrate that this nitrogen retention is not a kinetic phenomenon. The TGA curves may be slightly modified by the variation of heating rate or oxygen partial pressure. However, the thermogravimetric intermediate step position is independent of those parameters, moreover, the intermediate phases have an extremely high thermal stability. For example the transition temperature (Ts) between intermediate phase and final oxide reaches 930°C in the case of $Y_{2.67}W_{1.33}O_{3.79}N_{2.80}\square_{1.41}$ (Fig. 2(b)). Such a temperature is incompatible with nitrogen gas bubbles confined inside the solid lattice.

In addition to the oxynitride systems listed in Table 1, in which preparation of intermediate phases was performed, this nitrogen retention phenomenon was also observed in the following

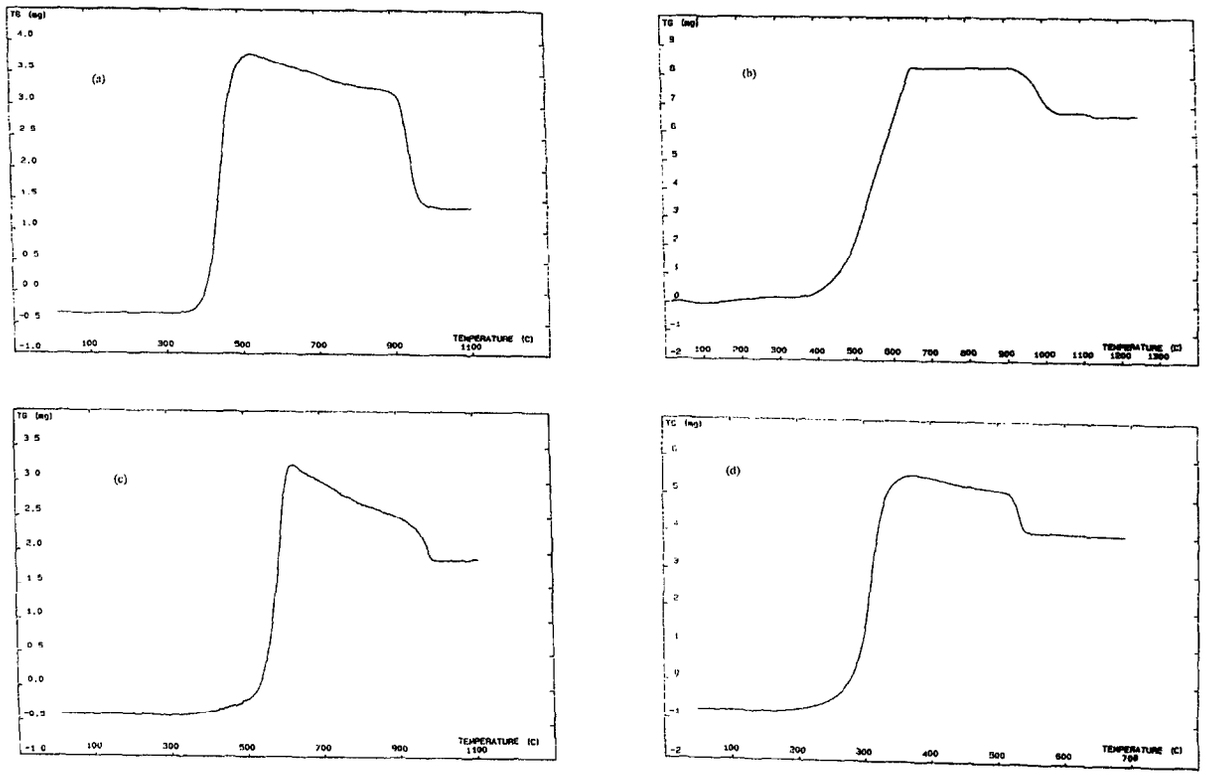

Fig. 2. TGA of $LaTiO_2N$(a), $Y_{2.67}W_{1.33}O_{3.79}N_{2.80}\square_{1.41}$ (b), $BaTaO_2N$ (c) and $Nb_{0.54}\square_{0.46}O_{0.4}N_{0.6}$ (d) under air (P = 1 atm) at 0·8 K mn^{-1}.

systems: Li–Ge–O–N; Cd–Ge–O–N; Ga–O–N (tetrahedral wurtzite-type structure); Nd–W–O–N, La–V–O–N (perovskite); Sr–Ta–O–N (K_2NiF_4 and perovskite types); Al–V–O–N (X-ray amorphous). This list is not exhaustive.

4 Intermediate Phase

4.1 Synthesis

Intermediate phases were isolated in significant amounts by isothermal treatment in air (P = 1 atm) of starting oxynitrides, in a tube furnace. In each case, the step temperature was chosen near threshold temperature in order to prevent any contamination by the oxide phase. Using this process, pure intermediate phases could be prepared after a long step time at the reaction temperature, except for the Ti–O–N phase in which presence of TiO_2 was always detected by XRD whatever the experimental conditions. The transformation was controlled by sample weighing, XRD and determination of nitrogen and oxygen content by LECO analysis. In each case, the sample composition after reaction corresponds to the top of the associated TGA curve. Synthesis conditions are indicated in Table 2. Note that all the reaction products are stable in ambient air.

4.2 Formulation

An intermediate phase produced from $BaTaO_2N$ precursor was heated in pure argon at a temperature (1000°C) higher than its transition temperature Ts (Fig. 1(b)). X-ray diffraction revealed the same powder pattern as by TGA in air, i.e. the formation of the same oxide phases. Moreover, high resolution mass-spectrometry only detected nitrogen (N_2) release. The type of formulation of the intermediate phase can be deduced from these results and taking into account the relative weight

Table 2. Intermediate phase synthesis conditions

Oxynitride precursor	*Intermediate phase synthesis temperature (°C)*	*Thermal treatment time (h)*
$BaTaO_2N$	580	50
$Y_{2.67}W_{1.33}(O_{3.79}N_{2.80}\square_{1.41})$	440	60
$Cr_{0.77}\square_{0.23}O_{0.69}N_{0.31}$	330	4
$Al_{2.85}\square_{0.15}O_{3.45}N_{0.55}$	860	50
$La_{0.91}W_{0.91}\square_{0.18}O_{1.37}N_{1.63}$	490	16
$Ti_{0.67}\square_{0.33}O_{0.42}N_{0.58}$	390	14
$LaTiO_2N$	470	50
$Nb_{0.54}\square_{0.46}O_{0.4}N_{0.6}$	325	40

loss of the TGA curve, the decomposition reaction is written as follows

$$\underset{\text{Intermediate phase}}{BaTaO_{3.5}N_{0.31}} \xrightarrow{1000°C \text{ under Ar}} \underset{\text{oxide}}{\text{'}BaTaO_{3.5}\text{'} + 0{\cdot}155N_2\uparrow}$$

The oxide phase obtained is in fact a mixture of $Ba_5Ta_4O_{15}$ and $BaTa_2O_6$. We generalize this decomposition behavior to all studied intermediate phases. (M^{n+} represents the whole cationic network.)

$$\underset{\text{Intermediate phase}}{M^{n+}O_{n/2}N_x} \xrightarrow{Ts} \underset{\text{oxide}}{M^{n+}O_{n/2} + x/2N_2\uparrow}$$

All the intermediate phase compositions deduced from TGA curves are given in Table 3. Unit cell content will be discussed later. They are in good agreement with the oxygen and nitrogen LECO measurements.

4.3 X-ray diffraction (XRD)

In most studied systems, the intermediate phase crystallizes in the same structure type as its oxynitride precursor. However, an amorphization is observed which, in some systems (La–W–O–N, Nb–O–N), is complete. In addition, a slight increase in the unit cell volume (less than 1%) can be noted for the Ba–Ta–O–N, Y–W–O–N and La–Ti–O–N systems. As an illustration, XRD spectra of (a) $BaTaO_2N$ and (b) $Ba_2Ta_2O_7NO_{0.62}$ are shown in Fig. 3, both with a perovskite unit cell.

4.4 Density measurements

Experimental density values are given in Table 4, for three couples oxynitride precursor of intermediate and associated phases. In each case, the density of the intermediate phase is significantly lower (up to 20%) than that of the starting oxynitride. Such a difference is independent of the density measurement method, even if this weakly underestimates the density value. This fact is quite surprising, *a priori*, since each intermediate phase is obtained with a weight gain from its precursor and without noticeable unit cell volume variation. This intermediate phase property will be discussed in the final section.

4.5 X-ray photoelectron spectroscopy (XPS) study

Table 5 displays the values of N1s binding energies of several intermediate phases and corresponding precursors (5(a) and (b)).

Table 3. Intermediate phase formulations

Oxynitride precursor		*Intermediate phase*	
Composition	*Structure type*	*Composition*	*Unit cell content*
$BaTaO_2N$	perovskite	$Ba_2Ta_2O_7N_{0.62}$	$Ba_{0.72}\square_{0.28}Ta_{0.72}\square_{0.28}O_{2.51}(N_2)_{0.11}\square_{0.38}$
$Y_{2.67}W_{1.33}(O_{3.79}N_{2.80}\square_{1.41})$	fluorite	$Y_2WO_6N_{0.40}$	$Y_{2.13}W_{1.06}\square_{0.81}O_{6.38}(N_2)_{0.21}\square_{1.41}$
$Cr_{0.77}\square_{0.23}O_{0.69}N_{0.31}$	NaCl	$Cr_2O_3N_{0.30}$	$Cr_{0.63}\square_{0.27}O_{0.95}(N_2)_{0.05}$ (*4)
$Al_{2.85}\square_{0.15}O_{3.45}N_{0.55}$	spinelle	$Al_2O_3N_{0.19}$	$Al_{2.59}\square_{1.41}O_{3.88}(N_2)_{0.12}$ (*8)
$Nb_{0.54}\square_{0.46}O_{0.4}N_{0.6}$	NaCl	$Nb_2O_5N_{0.86}$	$Nb_{0.37}\square_{0.63}O_{2.82}(N_2)_{0.18}$ (*4)
$LaTiO_2N$	perovskite	$La_2Ti_2O_7N_{1.28}$	$La_{0.79}\square_{0.21}Ti_{0.79}\square_{0.21}O_{2.75}(N_2)_{0.25}$
$La_{0.91}W_{0.91}\square_{0.18}O_{1.37}N_{1.63}$	perovskite	$La_2W_2O_9N_{0.94}$	$La_{0.63}\square_{0.27}W_{0.63}\square_{0.27}O_{2.85}(N_2)_{0.15}$
$Ti_{0.67}\square_{0.33}O_{0.42}N_{0.58}$	NaCl	$TiO_2N_{0.12}$	$Ti_{0.49}\square_{0.97}O_{0.51}(N_2)_{0.03}$ (*4)

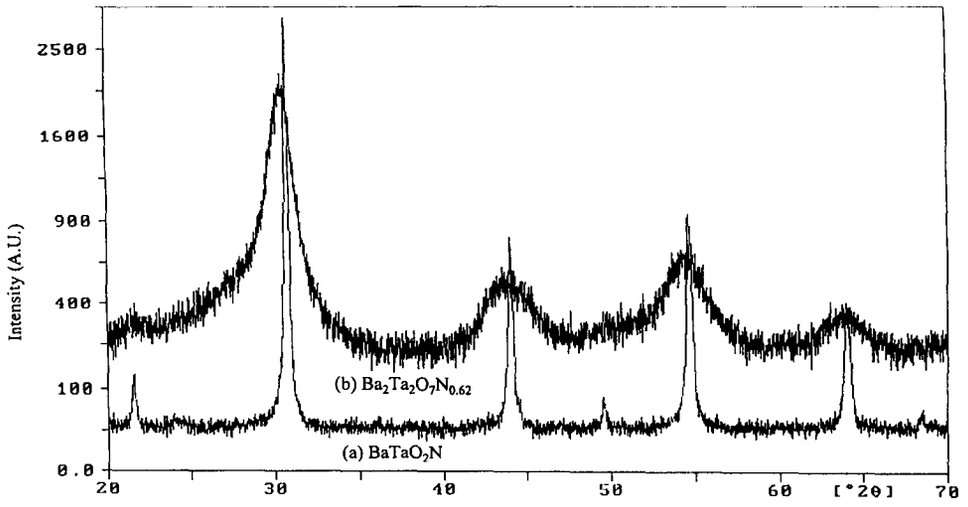

Fig. 3. XRD of (a) $BaTaO_2N$ and (b) $Ba_2Ta_2O_7N_{0.62}$.

Table 4. Densities of oxynitrides and associated intermediate phases

Oxynitride precursor/intermediate phase	*Density*
$Ba_{0.90}\square_{0.10}Ta_{0.90}\square_{0.10}O_{1.80}N_{0.90}\square_{0.30}$ (1)	7·9
$Ba_{0.72}\square_{0.28}Ta_{0.72}\square_{0.28}O_{2.51}(N_2)_{0.11}\square_{0.38}$	6·4
$Y_{2.67}W_{1.33}(O_{3.79}N_{2.80}\square_{1.41})$	6·8
$Y_{2.13}W_{1.06}\square_{0.81}\ O_{6.38}(N_2)_{0.21}\square_{1.41}$	5·5
$Al_{2.85}\square_{0.15}O_{3.45}\ N_{0.55}$	3·7
$Al_{2.59}\square_{1.41}O_{3.88}(N_2)_{0.12}$	3·4

(1) This formula corresponds to the previous $BaTaO_2N$ formulation, according to its density measurement.

Table 5. (a) Oxynitride precursors N1s binding energies

Oxynitride precursor	*N1s binding energy (eV)*	*FWHM (eV)*
$Ti_{0.67}\square_{0.33}O_{0.42}N_{0.58}$	396·7	1·6
$Nb_{0.54}\square_{0.46}O_{0.4}N_{0.6}$	396·9	1·6
$La_{0.91}W_{0.91}\square_{0.18}O_{1.37}N_{1.63}$	396·0	1·6
$Cr_{0.77}\square_{0.23}O_{0.69}N_{0.31}$	396·4	1·6
$Y_{2.67}W_{1.33}(O_{3.79}N_{2.80}\square_{1.41})$	396·3	1·6

Table 5. (b) Intermediate phase N1s binding energies

Intermediate phases	*N1s binding energy (eV)*	*FWHM (eV)*
$TiO_2N_{0.12}$	403·2	1·8
$Nb_2O_5N_{0.86}$	402·8 ⟺ 403·2	1·8
$La_2W_2O_9N_{0.94}$	403·3	1·8
$Cr_2O_3N_{0.30}$	402 ⟺ 402·3	1·8
$Y_2WO_6N_{0.40}$	403·0	1·8

The Nls peaks situated at 396·0⟺396·9 eV are characteristic of nitride N^{3-} species in agreement with the literature. The intermediate phase synthesis is accompanied by an important shift in N1s binding energy since they present values up to 403 eV, (the precise energy position is influenced by oxidation step and metal type involved).

4.6 Discussion

Such intermediate phase composition and particular nitrogen binding type determined by XPS induce an interaction of metal–nitrogen at the near zero oxidation step. In organometallic chemistry, several complexes[11,12] can be found which show different binding modes, but the most frequently observed is linear (end-on): M–N≡N–M. Part of those complexes have been studied by XPS (Table 6). Nitrogen binding energies are function of the ligand type and of the complex geometry. The different co-ordination modes, $M(N_2)$ or $M(N_2)_2$, of XPS-studied complexes involve a multiplet Nls signal. N1s binding energies associated with these dinitrogen species are in the range 401·4–403 eV.

On the other hand, by low energy implantation (N_2^+ bombardment) of TiO_2 layers, Milosev *et al.*[18] and Wolff *et al.*[19] have shown that part of implanted nitrogen exists as molecular N_2. The other part of nitrogen is represented by nitride species N^{3-}. A peak in the range 402·5–403·7 eV is ascribed to those N_2 entities in interaction with TiO_2 lattice. Electrochemical reoxidation of such films shows an increase of the Nls XPS surface peak near 403 eV associated to the N^{3-}/N_2 transformation. In the same way, dinitrogen complexes[20] of aluminum have been isolated at alumina/AlN interface. Those dinitrogen species, characterized by an XPS Nls peak near 401 eV, are a partial result of the reaction between trimethylaluminum and ammonia on alumina at 600 K.

All these results are indications that, in the intermediate phases $M^{n+}O_{n/2}N_x$, metal–nitrogen interaction corresponds to an organometallic type: M–N≡N–M.

This suggests the following oxidation process of the oxynitride precursor: part of the nitrogen leaves the lattice as molecular dinitrogen and is replaced by incoming oxygen which locates in normal anionic positions. The remaining nitrogen forms dinitrogen bridges between metallic atoms. N–N or M–N bond lengths encountered in organometallic complexes are compatible with the lattice oxide. This model involves the creation of cationic vacancies in order to simultaneously respect metal–oxide stoichiometry and lattice crystal type determined by XRD. The resulting unit cell content is given in Table 3. Assuming that the amount of anionic vacancies does not change, our notation effectively induces an important

Table 6. N1s binding energies of dinitrogen complexes

Complexes	*N°*	*XPS N1s binding energy (eV)*			*Ref.*
$PdCl_2((PhCH_2)Me_2NNCOPh)_2$	1	401·4		398·5	13
$PdCl_2(R^1R^2R^3NNCOR^4)_2$	2	402–402·5	400·0 (NH)	396·9–398·5	14
M–N=N–Ar	3	endo 401·7	exo 400·6		15
$Ir^{3+}(NH_2CH_2COO^-)_2(NH_3CH_2COO^-)$	4	402·2	400·4		16
$(RuCl(N_2)(diars)_2)SbF_6$	5	402·3	400·7		17
$Mn(\eta\text{-}C_5H_5)(CO)_2(N_2)$	6	403·0	401·8		17

decrease of the powder density during the intermediate phase synthesis (Table 4).

Our model does not give, at present, all the answers to all the questions concerning the oxidation states of the different anionic and cationic elements involved. For example, in the Al/O/N system, aluminum is trivalent in the starting oxynitride and this state (+3) cannot change during its thermal treatment under oxygen. In the intermediate phase, that we have written as $Al_2O_3N_{0.19}$, oxygen, according to its Ols XPS signal, is still formally (−2). Therefore, even if nitrogen is present as M–N≡N–M, we must associate a weak negative charge to this NN species: $N_2^{\alpha-}$. Consequently, the only coherent intermediate phase notation would be: $M^{n+}O^{2-}_{(n/2)-(\alpha x/2)}\ (N_2^{\alpha-})_x$. According to the organometallic literature and to our formulation, n/2 is much higher than $\alpha x/2$. This fact explains why we cannot detect associated oxygen vacancies in the oxide phase obtained by intermediate phase decomposition under argon. Complementary studies are planned and in this first approach we will keep this $M^{n+}O_{n/2}N_x$ notation.

5 Conclusion

Oxidation of transition metal oxynitrides with defect structure leads to new compounds $M^{n+}O_{n/2}N_x$ called intermediate phases. XPS N1s of this nitrogen retention reveals a nitrogen type of bonding very close to the one encountered in organometallic dinitrogen complexes.

Acknowledgements

The authors would like to thank E. Gueguen and P. Grange of the University of Louvain La Neuve (Belgium) and P. Goeuriot of the Ecole des Mines de St Etienne (France) for XPS measurements and helpful discussions.

References

1. Goursat, P., Billy, M., Goeuriot, P., Labbe, J. C., Villechenoux, J. M., Roult, G. and Bardolle, J. *Journal Mater. Chem.*, 1981, **6**, 81.
2. Veyret, J. B., Vandevoorde, M. and Billy, M. *Journal Am. Ceram. Soc.*, 1992, **75**, 3289.
3. Wang, X. H., Lejus, A. M. and Vivien, D. *Journal Am. Ceram. Soc.*, 1990, **73**, 770.
4. Le Gendre, L., Marchand, R., Laurent, Y., Gueguen, E. and Grange, P. *Eur. Journal Solid. State Inorg Chem.*, to be published.
5. Pors, F., Marchand, R., Laurent, Y., Bacher, P. and Roult, G. *Mater. Res. Bull.*, 1988, **23**, 1447.
6. Bacher, P., Antoine, P., Marchand, R., L'Haridon, P., Laurent, Y. and Roult, G. *Journal Solid. State Chem.*, 1988, **77**, 67.
7. Marchand, R., Pors, F. and Laurent, Y. *Ann. Chim. Fr.*, 1991, **16**, 553.
8. Marchand, R., Antoine, P. and Laurent, Y. *Journal Solid. State Chem.*, 1993, **107**, 34.
9. Gouin, X., Le Gendre, L., Marchand, R. and Laurent, Y. *Ann. Chim. Fr.*, 1995, **20**, 293.
10. Kim, H. S., Sayag, C., Bugli, G., Djega-Mariadassou, G. and Boudart, M., *Mat. Res. Soc. Symp. Proc.*, 1995, **368**, 3.
11. Blomberg, M. R. A., Siegbahn, P. E. M. *Journal Amer. Chem. Soc.*, 1993, **115**, 6908.
12. Hidai, M. and Mizobe, Y. *Chem. Rev.*, 1995, **95**, 1115.
13. Seno, M. and Tsuchiya, S. *Journal Chem. Soc., Dalton Trans.*, 1977, 751.
14. Seno, M. and Tsuchiya, S. *Journal Chem. Soc., Dalton. Trans.*, 1984, 731.
15. Brandt, P. and Feltham, R. D. *Journal Organomet. Chem.*, 1976, **120**, C53.
16. Srivastava, S. *Appl. Spectrosc. Rev.*, 1986, **22**, 401.
17. Chatt, J., Da Câmara Pina, L. M. and Richards, R. L., *New Trends in the Chemistry of Nitrogen Fixation*, Academic Press Inc., 1980.
18. Milosev, I., Strehblow, H. H., Navinsek, B. and Metikos-Hokovic, M. *Surf. Interf. Analysis*, 1995, **23**, 529.
19. Wolff, M., Schultze, J. W. and Strehblow, H.H. *Surf. Interf. Analysis*, 1991, **17**, 726.
20. Liu, H., Bertolet, D. C. and Rogers, J.W. *Surf. Sci.*, 1995, **340**, 88.